

Final Results of the GEp-III Experiment and the Status of the Proton Form Factors

A. J. R. Puckett*

*Los Alamos National Laboratory,
Los Alamos, NM 87544, U. S. A.*

**E-mail: puckett@lab.org
www.lanl.gov*

The GEp-III Collaboration

*Thomas Jefferson National Accelerator Facility,
Newport News, VA 23606*

The recently published final results of experiment E04-108 in Jefferson Lab Hall C extend the recoil polarization measurements of the ratio of the proton electric and magnetic form factors to $Q^2 = 8.5 \text{ GeV}^2$, an increase in Q^2 coverage of more than 50%. A global fit of G_E^p and G_M^p to selected data for electron-proton elastic scattering cross sections and polarization observables is presented, illustrating the statistical impact of the new results.

Keywords:

The elastic electromagnetic form factors of the nucleon are among the most fundamental quantities describing its structure. In the one-photon-exchange or Born approximation, the helicity-conserving Dirac form factor $F_1(Q^2)$ and the helicity-flip Pauli form factor $F_2(Q^2)$ fully characterize the amplitude for elastic electron-nucleon scattering at a spacelike momentum transfer $Q^2 = -q^2 > 0$. These form factors are accessible experimentally through both cross section and double-polarization measurements, and are often expressed in terms of the equivalent linear combinations $G_E = F_1 - \tau F_2$ (electric) and $G_M = F_1 + F_2$ (magnetic), which are more readily extracted from experimental observables. The Born differential cross section for elastic ep

scattering is given by¹

$$\begin{aligned} \frac{d\sigma}{d\Omega_e} &= \frac{\alpha^2}{Q^2} \left(\frac{E'_e}{E_e} \right)^2 \cot^2 \frac{\theta_e}{2} \frac{G_E^2 + \frac{\tau}{\epsilon} G_M^2}{1 + \tau} \\ &= \frac{\sigma_{Mott}}{\epsilon(1 + \tau)} [\epsilon G_E^2 + \tau G_M^2] \end{aligned} \quad (1)$$

where α is the fine-structure constant of electromagnetism, E_e and E'_e are the lab incident and scattered electron energies, θ_e is the lab electron scattering angle, $\tau = Q^2/4M^2$, M is the nucleon mass, and $\epsilon = [1 + 2(1 + \tau) \tan^2 \frac{\theta_e}{2}]^{-1}$ corresponds to the longitudinal polarization of the virtual photon in the single-photon-exchange picture.

The polarization of protons scattered elastically by longitudinally polarized electrons has nonvanishing longitudinal and transverse components relative to the momentum transfer in the scattering plane given by^{2,3}

$$I_0 P_l = \sqrt{\tau(1 + \tau)} \tan^2 \frac{\theta_e}{2} \frac{E_e + E'_e}{M} G_M^2, \quad (2)$$

$$I_0 P_t = -2\sqrt{\tau(1 + \tau)} \tan \frac{\theta_e}{2} G_E G_M, \quad (3)$$

where $I_0 = G_E^2 + \frac{\tau}{\epsilon} G_M^2$. The component P_n normal to the scattering plane is exactly zero in the Born approximation. The ratio P_t/P_l is directly proportional to G_E/G_M :

$$R = \mu_p \frac{G_E^p}{G_M^p} = -\mu_p \frac{P_t}{P_l} \frac{E_e + E'_e}{2M} \tan \frac{\theta_e}{2} \quad (4)$$

The ratio (4) provides enhanced sensitivity to G_E at large Q^2 , where G_M dominates the cross section (see equation (1)). Precise recoil polarization experiments⁴⁻⁶ first established that R decreases rapidly with $Q^2 \geq 1 \text{ GeV}^2$, in strong disagreement with cross section measurements. The extraction of a small G_E^2 term compared to a dominant $\frac{\tau}{\epsilon} G_M^2$ term from L/T separation measurements becomes highly sensitive to incompletely understood higher-order QED effects at large Q^2 , including two-photon exchange (TPEX).⁷ The enhanced sensitivity of the recoil polarization method to G_E and the typically smaller relative importance of radiative corrections and TPEX to the ratio (4) have led to a general consensus that the polarization data most reliably determine G_E^p at large Q^2 .

Extending the accurate measurements of the proton and neutron electric and magnetic form factors to the highest accessible Q^2 provides crucial experimental input to understanding the transition between the non-perturbative and perturbative regimes of QCD. In addition to constraining

QCD-inspired phenomenological models, precise form factor data provide important model-independent information about the structure of the nucleon. The recently published results of experiment E04-108⁸ in Jefferson Lab's Hall C extended the recoil polarization data for R to $Q^2 = 8.5 \text{ GeV}^2$. In this paper we illustrate the statistical impact of the new data in a global fit to elastic electron-proton scattering data, including both cross section and polarization measurements, using the Kelly parametrization⁹ of G_E^p and G_M^p .

The Kelly parametrization of the nucleon form factors⁹ is given by the ratio of a polynomial of order n to a polynomial of order $n + 2$ in $\tau = Q^2/4M^2$:

$$G(Q^2) = \frac{\sum_{k=0}^n a_k \tau^k}{1 + \sum_{k=1}^{n+2} b_k \tau^k} \quad (5)$$

This parametrization satisfies $G(Q^2) \propto Q^{-4}$ as $Q^2 \rightarrow \infty$ and gives the appropriate static ($Q^2 \rightarrow 0$) limit if one fixes $a_0 = 1$ for G_E^p and G_M^p/μ_p . This parametrization is chosen to have the large- Q^2 behavior expected from dimensional scaling laws in perturbative QCD.^{10,11} The original 2004 analysis by Kelly using this parametrization found that a four-parameter fit with $n = 1$ could describe the data for G_E^p and $G_M^{p,n}$ with a reasonable χ^2 . For simplicity's sake, the results presented here use the same choice.

The published elastic ep scattering data chosen for the fit include 421 differential cross section measurements spanning $0.005 \text{ GeV}^2 \leq Q^2 \leq 31.2 \text{ GeV}^2$ and 53 polarization measurements spanning $0.162 \text{ GeV}^2 \leq Q^2 \leq 8.49 \text{ GeV}^2$. The differential cross section data were taken from Refs. 12–23, while the polarization data were taken from Refs. 5,6,8,24–30. While by no means comprehensive, the chosen data are sufficiently representative of the precision and Q^2 coverage of all elastic ep scattering data. All data included in this analysis were obtained from hydrogen targets.

The best fit parameters for G_E^p and G_M^p were obtained in a simultaneous global analysis of cross section and polarization data by minimizing the χ^2 function defined as

$$\chi^2 = \sum_{i=1}^{N_\sigma} \left[\frac{\sigma_{R,data}^{(i)} - (\epsilon G_E^2 + \tau G_M^2)^{(i)}}{\Delta \sigma_{R,data}^{(i)}} \right]^2 + \sum_{i=1}^{N_{pol.}} \left[\frac{R_{p,data}^{(i)} - R_p^{(i)}}{\Delta R_{p,data}^{(i)}} \right]^2, \quad (6)$$

where $R_p = \mu_p G_E^p/G_M^p$, G_E^p and G_M^p/μ_p are given by the formula (5) with $n = 1$ and $a_0 = 1$, $a_1^{E,M}$ and $b_{1,2,3}^{E,M}$ are eight adjustable parameters to be determined, $\sigma_{R,data} = \epsilon(1 + \tau)\sigma_{data}/\sigma_{Mott}$ (see equation (1)), and $\Delta \sigma_{R,data}$ and $\Delta R_{p,data}$ are the uncertainties in the experimental data. For the cross

section data, statistical uncertainties and overall normalization uncertainties, when quoted with the published results, were included in $\Delta\sigma_{R,data}$. For the polarization data, only statistical uncertainties were included.

The inconsistency between the Rosenbluth and polarization data for $Q^2 \geq 1 \text{ GeV}^2$ was handled using an iterative procedure. Three iterations of the fit were performed. For all cross section data with $Q^2 \geq 1 \text{ GeV}^2$, the value of G_E^p in equation (6) was replaced by a fixed value of G_E^p calculated from the results of the previous fit, or, in the case of the first iteration, using the results of Kelly’s 2004 analysis.⁹ This replacement has the effect that for $Q^2 \geq 1 \text{ GeV}^2$, G_E^p is entirely determined by polarization data, while G_M^p is determined by cross section data, with G_E^p fixed by the polarization data for R_p . For $Q^2 < 1 \text{ GeV}^2$, cross section and polarization data are treated on an equal footing for both G_E^p and G_M^p . The numerical minimization was carried out using the TMinuit class within the ROOT libraries.³¹ Typically, no significant improvement of the fit was found after two iterations of the starting function for G_E^p .

This fit procedure was performed for two data sets identical in every respect except that the new JLab Hall C data for R_p were excluded from the first data set and included in the second set. Table 1 shows the results

Table 1. Fit results for G_E^p and G_M^p/μ_p , with (“Old”) and without (“New”) the data of Ref. 8. $G_\infty/G_D = 16M_p^4/\Lambda^2 (a_1/b_3)$ is the asymptotic value of G_E^p/G_D and $G_M^p/(\mu_p G_D)$. The “standard” dipole form factor is defined as $G_D = (1 + Q^2/\Lambda^2)^{-2}$, with $\Lambda^2 = 0.71 \text{ GeV}^2$.

	Old G_E^p	Old G_M^p	New G_E^p	New G_M^p
a_1	$-.390 \pm .081$	$.075 \pm .023$	$-.299 \pm .072$	$.081 \pm .023$
b_1	$11.01 \pm .10$	$11.14 \pm .08$	$11.11 \pm .09$	$11.15 \pm .08$
b_2	$13.57 \pm .84$	$18.44 \pm .16$	$14.11 \pm .83$	$18.45 \pm .16$
b_3	11.4 ± 4.5	$5.12 \pm .65$	15.7 ± 4.2	$5.31 \pm .66$
G_∞/G_D	$-.84 \pm .49$	$.360 \pm .064$	$-.47 \pm .23$	$.376 \pm .061$
$Q^2(G_E^p = 0)$	9.0		11.8	

of the fit with and without the new Jefferson Lab results. The parameter errors quoted are the standard errors calculated from the diagonal elements of the covariance matrix. Significant correlations among the parameters for each form factor were found. These correlations imply that the uncertainties in the asymptotic form factor values and the uncertainties in G_E^p and G_M^p at any given Q^2 cannot be calculated directly from the parameter errors, but instead require the full covariance matrix. On the other hand, the correlation coefficients between the parameters describing G_E^p and those

describing G_M^p were generally small, at the level of a few percent. Table 2 shows the asymptotic values of $Q^6 F_2^p$ and $Q^4 F_1^p$ for the fits with and without the new high Q^2 data.

Table 2. Asymptotic values of $Q^4 F_1$ and $Q^6 F_2$, with and without Ref. 8.

Old $Q^6 F_{2,\infty}^p$	New $Q^6 F_{2,\infty}^p$	Old $Q^4 F_{1,\infty}^p$	New $Q^4 F_{1,\infty}^p$
$3.28 \pm .93$	$2.69 \pm .51$	$.507 \pm .090$	$.529 \pm .086$

Table 3 illustrates the quality of the fit in terms of χ^2 . Although the overall χ^2 of the fit $\chi^2/n.d.f. = 828.4/466 = 1.78$ might be regarded as relatively poor, the extent to which the reduced χ^2 exceeds one per datum reflects the inconsistency between the Rosenbluth and polarization methods, as shown in table 3. The polarization data and the cross section data for $Q^2 \leq 1 \text{ GeV}^2$ are consistent with the fit results for G_E^p and G_M^p . Relative to the number of data points, the cross section data for $1 \leq Q^2 \leq 10 \text{ GeV}^2$ contribute disproportionately to χ^2 , since the ϵ -dependence of the measured cross sections disagrees with the slope predicted by the polarization data.

Table 3. χ^2 of the final global fit with new data included.

Observable	N_{data}	χ^2
$\sigma_R, Q^2 \leq 1 \text{ GeV}^2$	269	293.8
$\sigma_R, 1 < Q^2 \leq 10 \text{ GeV}^2$	142	483.3
$\sigma_R, Q^2 > 10 \text{ GeV}^2$	10	3.96
$R_p^{pol.}, \text{ all } Q^2$	53	47.4
All data	474	828.4

Figures 1 and 2 show the fit results together with the experimental data. In figure 1(a), polarization data for R_p were converted to G_E^p data using the fit result for G_M^p and appropriate error propagation. The best fit curves are shown with standard 1σ uncertainty bands calculated from the full covariance matrix. As shown in figure 1(a), the new G_E^p data⁸ favor a slowing rate of decrease of G_E^p with Q^2 compared to previous data, and shrink the uncertainty in G_E^p for $Q^2 \geq 5 \text{ GeV}^2$ by roughly a factor of two. The improved constraint on F_2^p in the high- Q^2 region shown in figure 1(b) is similarly dramatic.

Figure 2 shows the results for $G_M^p/\mu_p G_D$ and $Q^4 F_1^p$. The interesting feature of the G_M^p results is that the fit is systematically higher than the published data in the region of the discrepancy. Since the cross section

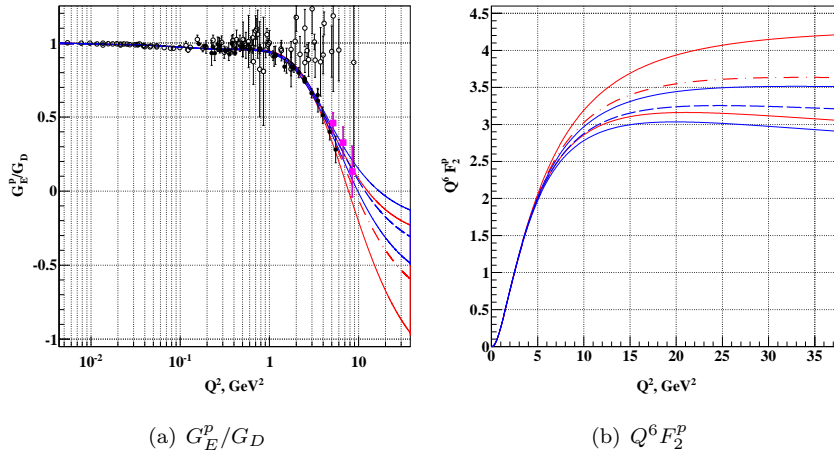


Fig. 1. Fit results for G_E^p/G_D^p (a), and $Q^6 F_2^p$ (b), before (red dot-dashed) and after (blue dashed) including the results of Ref. 8, with 1σ uncertainty bands. Published values of G_E^p extracted from cross section (open circles) and polarization (filled circles) measurements. Results of Ref. 8 (magenta squares).

measurements either extracted or assumed $R_p \approx 1$, the contribution of G_E^p to σ_R was overestimated, lowering the extracted values of G_M^p . This result for G_M^p is quantitatively and qualitatively similar to the result of a recent global analysis including TPEX corrections to the cross section data.³² In contrast to this analysis, which neglects TPEX completely, the authors of Ref. [32] used the Kelly parametrization with $n = 3$ and achieved a substantially better χ^2 , since the applied TPEX corrections largely reconciled the discrepancy. Although the new R_p data barely affect G_M^p and its uncertainty, the effect on F_1^p is more significant, an entirely expected result given the dramatic improvement in F_2^p and the definition $G_M = F_1 + F_2$. For yet larger Q^2 , the fit result for G_M^p again agrees with the published data, reflecting the dominance of σ_R by G_M^p , shown in figure 3.

In conclusion, new high Q^2 measurements of $R = \mu_p G_E^p/G_M^p$ in Jefferson Lab's Hall C have significantly extended the range of Q^2 for which G_E^p is accurately determined. The impact of these new data on the world database of proton form factors was studied in the context of an empirical parametrization with physically reasonable assumptions for low and high Q^2 asymptotic behavior; i.e., $G_E^p(0) = 1$ and $G_M^p(0) = \mu_p$, and $F_{1(2)}^p \propto Q^{-4(6)}$ as $Q^2 \rightarrow \infty$. In this context, the new data for R_p reduce the uncertainty in G_E^p by roughly a factor of two in the measured Q^2 region and in the ex-

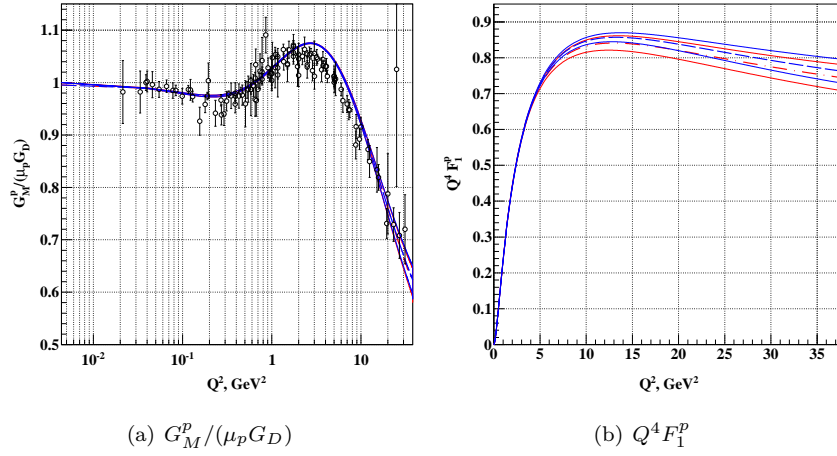


Fig. 2. Fit results for $G_M^p / (\mu_p G_D)$ (a) and $Q^4 F_1^p$ (b), before (red dot-dashed) and after (blue dashed) including the results of Ref. 8. Published values of G_M^p extracted from cross section (open circles) measurements.

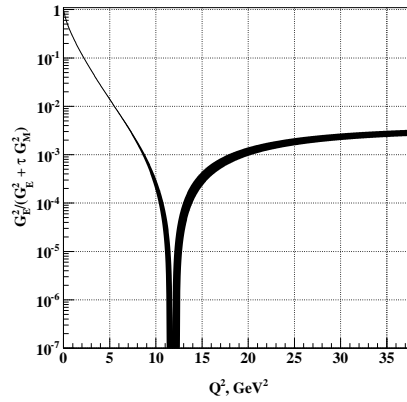


Fig. 3. $G_E^2 / (G_E^2 + \tau G_M^2)$, calculated from the results of the global fit, represents the maximum fraction of the reduced cross section carried by G_E .

trapolation to higher Q^2 . Looking to the future, planned recoil polarization measurements of R_p to $Q^2 \approx 15 \text{ GeV}^2$ and precision elastic ep differential cross section measurements to $Q^2 \approx 18 \text{ GeV}^2$ using JLab's upgraded 11 GeV electron beam will complete the experimental knowledge of proton electromagnetic form factors in the spacelike region attainable with present

day accelerators.

References

1. M. N. Rosenbluth, *Phys. Rev.* **79**, p. 615 (1950).
2. A. I. Akhiezer and M. P. Rekalo, *Sov. J. Part. Nucl.* **3**, p. 277 (1974).
3. R. G. Arnold, C. E. Carlson and F. Gross, *Phys. Rev. C* **23**, p. 363 (1981).
4. M. K. Jones *et al.*, *Phys. Rev. Lett.* **84**, p. 1398 (2000).
5. V. Punjabi *et al.*, *Phys. Rev. C* **71**, p. 055202 (2005).
6. O. Gayou *et al.*, *Phys. Rev. Lett.* **88**, p. 092301 (2002).
7. C. E. Carlson and M. Vanderhaeghen, *Annu. Rev. Nucl. Part. Sci.* **57**, p. 171 (2007).
8. A. J. R. Puckett *et al.*, *Phys. Rev. Lett.* **104**, p. 242301 (2010).
9. J. J. Kelly, *Phys. Rev. C* **70**, p. 068202 (2004).
10. S. J. Brodsky and G. R. Farrar, *Phys. Rev. D* **11**, p. 1309 (1975).
11. G. P. Lepage and S. J. Brodsky, *Phys. Rev. Lett.* **43**, p. 545 (1979).
12. T. Janssens *et al.*, *Phys. Rev.* **142**, p. 922 (1966).
13. C. Berger *et al.*, *Phys. Lett. B* **35**, p. 87 (1971).
14. L. E. Price *et al.*, *Phys. Rev. D* **4**, p. 45 (1971).
15. W. Bartel *et al.*, *Nucl. Phys. B* **58**, p. 429 (1973).
16. P. N. Kirk *et al.*, *Phys. Rev. D* **8**, p. 63 (1973).
17. F. Borkowski *et al.*, *Nucl. Phys. A* **222**, p. 269 (1974).
18. F. Borkowski *et al.*, *Nucl. Phys. B* **93**, p. 461 (1975).
19. G. G. Simon *et al.*, *Nucl. Phys. A* **333**, p. 381 (1980).
20. A. F. Sill *et al.*, *Phys. Rev. D* **48**, p. 29 (1993).
21. L. Andivahis *et al.*, *Phys. Rev. D* **50**, p. 5491 (1994).
22. M. E. Christy *et al.*, *Phys. Rev. C* **70**, p. 015206 (2004).
23. I. A. Qattan *et al.*, *Phys. Rev. Lett.* **94**, p. 142301 (2005).
24. M. J. Alguard *et al.*, *Phys. Rev. Lett.* **37**, p. 1258 (1976).
25. B. D. Milbrath *et al.*, *Phys. Rev. Lett.* **80**, p. 452 (1998).
26. T. Pospischil *et al.*, *Eur. Phys. J. A* **12**, p. 125 (2001).
27. O. Gayou *et al.*, *Phys. Rev. C* **64**, p. 038202 (2001).
28. C. Crawford *et al.*, *Phys. Rev. Lett.* **98**, p. 052301 (2007).
29. M. K. Jones *et al.*, *Phys. Rev. C* **74**, p. 035201 (2006).
30. G. Ron *et al.*, *Phys. Rev. Lett.* **99**, p. 202002 (2007).
31. R. Brun and F. Rademakers, *Nucl. Inst. and Meth. in Phys. Res. A* **389**, p. 81 (1997).
32. J. Arrington, W. Melnitchouk and J. A. Tjon, *Phys. Rev. C* **76**, p. 035205 (2007).